ORIGINAL RESEARCH

Assessment of OCT-Based Macular Curvature and Its Relationship with Macular Microvasculature in Children with Anisomyopia

Yue Wu · Xin Liu · Yuying Liu · Wenzhe Qian · Liandi Huang · Yixiang Wu ·

Xuetong Wang · Ying Yuan · Bilian Ke

ABSTRACT

Introduction: To evaluate the intraocular differences in optical coherence tomography (OCT)-based macular curvature index (MCI) among children with anisomyopia and to investigate the relationship between MCI and the macular microvasculature.

Methods: Fifty-two schoolchildren with anisometropia > 2.00 D were enrolled and underwent comprehensive examinations including cycloplegic refraction, axial length (AL), and swept source OCT/OCT angiography. OCT-based MCIs were determined from horizontal and vertical B-scans by a customized curve fitting model in MATLAB R2022 at 1-mm-, 3-mm-, and 6-mm-diameter circles at fovea. Characteristics and topographic variation of MCI was analyzed, and the relationships with microvascularity and its associated factors were investigated.

Results: MCI achieved high reliability and repeatability. There were overall larger MCIs in the more myopic eyes than the less myopic eyes in 1-mm-, 3-mm-, and 6-mm-diameter circles at fovea (all $p < 0.001$). For the topographic variation, horizontal MCI was significantly greater than vertical MCI (all $p < 0.001$), and was the largest in 6-mm circle, followed by 3-mm and 1-mm circles. Stronger correlation of horizontal MCI with myopic severity than vertical MCI was found. Partial Pearson's correlation found MCI was negatively associated with deep capillary plexus (DCP) vessel density ($p = 0.016$). Eyes with a higher MCI in a 6-mm circle were more likely to have longer AL ($p < 0.001$), lower DCP vessel density ($p = 0.037$), and thinner choroidal thickness (ChT) ($p = 0.045$).

Conclusion: Larger MCI was found in the more myopic eyes of children with anisomyopia and was significantly associated with smaller DCP density, suggesting that MCI was an important indicator of myopia-related retinal microvascularity change, and it could be a valuable metric for myopia assessment in children.

Y. Wu · X. Liu · Y. Liu · W. Qian · L. Huang · Y. Wu · X. Wang · Y. Yuan · B. Ke (✉)
Department of Ophthalmology, Shanghai General Hospital, Shanghai Jiao Tong University School of Medicine, No. 100 Haining Road, Hongkou District, Shanghai, China
e-mail: kebilian@126.com

Y. Wu · X. Liu · Y. Liu · W. Qian · L. Huang · Y. Wu · X. Wang · Y. Yuan
National Clinical Research Center for Eye Diseases, Shanghai, China

B. Ke
Department of Ophthalmology, Renji Hospital Affiliated to Shanghai Jiaotong University School of Medicine, Shanghai, China

Key Summary Points
Why carry out this study:
The global increase in myopia and its vision-threatening complications highlights the necessity of investigating macular shape.
Macular curvature has gained increasing attention in pathological adult myopia. However, little is known about its characteristics in children without high myopia or its associated factors.
Our study aimed to bridge these gaps by evaluating optical coherence tomography (OCT)-based macular curvature index (MCI) in children with anisomyopia with low to moderate myopia and exploring its relationship with macular microvasculature and other factors.
What was learned from the study?
In this study of children with anisomyopia, we demonstrated larger MCI in the more myopic eyes than the less myopic eyes and a significant negative correlation between MCI and deep capillary plexus (DCP) vessel density
Axial length, DCP vessel density, and choroidal thickness were independent factors associated with MCI in a 6-mm-diameter circle
We recommended MCI of OCT scans to evaluate the macular morphology as well as an indicator of microvascularity loss, and it could be a valuable metric for myopia assessment in clinical practice

INTRODUCTION

Myopia has witnessed a significant global increase in prevalence among children and adolescents [1, 2]. Extensive evidence has confirmed that myopic eyes change from generally oblate or spherical shape to a prolate ellipsoid [3–6]. In this context, macula also become out-pouched during myopia, a deformity in the macular region that has been associated with fundus degeneration and subsequent vision loss [7–12]. Considering the increasing myopia prevalence and its vision-threatening complications, evaluating the macular morphology is of great importance. Although macular shape has been previously described by depth, width, and volume [13–16], these metrics were oversimplified, and it was difficult to provide a complete description of the three-dimensional macular morphology from a single viewpoint.

In recent years, there has been a growing focus on macular curvature [17–24]. Macular curvature serves as a reflection of how the retina surface is contoured or curved in two dimensions, and it offers a more comprehensive understanding of retina anatomy and function atlas together with thickness and vascularity. Recent studies have investigated the relationship between macular curvature and ocular diseases. Wakazono et al. reported a time-dependent curvature increase in highly myopic adults and found it useful to predict the occurrence of posterior staphyloma [20]. Another study by them found that the difference in macular curvature between 3-mm-diameter circles and 3- to 6-mm rings was sufficient to distinguish the eyes with myopic traction maculopathy from simple highly myopic eyes [25]. Although it was suggested that highly myopic eyes had protruding eye shape and asymmetrical macular curvature in adults, to the best of our knowledge, few studies have further systemically quantified curvature changes in children, especially in children without high myopia without complications. Whether a similar pattern of curvature changes occurred in the early stages of myopia and at an early age remains unknown. It is imperative to explore macular curvature alterations and their association with myopia in children to assess its potential role as a myopia biomarker.

For the past decade, optical coherence tomography (OCT)/OCT angiography (OCTA) has enabled noninvasive imaging of the microvasculature alongside macular morphology simultaneously. Although previous studies have

attempted to correlate macular curvature with biometrics such as axial length, the results have been inconsistent [17, 21, 26], possibly because of the significant inter-individual variability and confounding effect in age, gender, genotype, and environment. Moreover, the association of macular curvature with macular microvascularity represents a significant gap in our current understanding. Decreasing retinal vascular plexus density has been reported in myopic eyes; however, the effect of macular curvature on macular microvasculature in retinal tissue remains to be determined.

Our study aimed to address these gaps by evaluating OCT-based macular curvature index (MCI) in children with anisomyopia with low to moderate myopia and exploring its relationship with macular microvasculature and other factors. By comparing the more myopic eye to the less myopic eye within the same individual, we can conduct a controlled and precise evaluation and investigate subtle difference in mild to moderate myopia. This approach will help determine the value of MCI as a myopia-related indicator in Chinese children, enhance our understanding of the underlying pathophysiology of myopia and may facilitate better prevention and treatment.

METHODS

Participants

The study protocol was approved by the ethics committee of Shanghai General Hospital, Shanghai Jiao Tong University (approval number 2022KY038) and was conducted in accordance with the Helsinki Declaration. Written informed consent was obtained from all participants and their guardians. In this study, anisometropic children aged 6–18 years old were recruited and examined between January 2021 and July 2022.

The inclusion criteria were as follows: (1) aged 6–18 years old; (2) best-corrected visual acuity of $>20/25$ in each eye to exclude amblyopia; (3) an intraocular spherical equivalent refraction difference of at least 2.00 D [27]. The exclusion criteria included: (1) high myopia (defined as spherical equivalent refraction >-6.00 D of either eye); (2) strabismus; (3) astigmatism (>2.00 diopter); (4) intraocular pressures (>21 mmHg); (5) history of ocular surgery; (6) any kind of ophthalmic disease or systemic disease that can affect the ocular structure and microvasculature, such as glaucoma, myopic maculopathy, retinopathy of prematurity, and so on; (7) history of atropine eye drops or use of orthokeratology within 3 months; (8) intake of coffee or alcohol within 24 h before the visit. Finally, 52 children were included in this study.

Ocular Examinations

All the participates who completed a standardized questionnaire underwent comprehensive ocular examinations including slit-lamp biomicroscopy, intraocular pressure measurement, and automatic cycloplegic refraction performed by a skilled senior optometrist. Spherical equivalent refraction (SER), which was calculated as spherical dioptric power plus half of cylindrical dioptric power, was used to represent refractive error. Corneal diameter (CR), central corneal thickness (CCT), anterior chamber depth (ACD), and axial length (AL) were measured by Pentacam-AXL (OCULUS, Germany). After that, swept source OCT/OCTA (SS-OCT/OCTA) was acquired. All these measurements were taken between 13:30–17:00 to avoid the potential influence of diurnal variation.

SS-OCT/OCTA Image Acquisition and Analysis

SS-OCT/OCTA images were conducted by VG200 (SVision imaging, China) using the three-dimensional 6×6 mm^2 macular volume scan mode, with a raster scan protocol of 512 (horizontal)$\times$512 (vertical) B-scans. The OCT used a 1050-nm wavelength laser with a scanning speed of 200,000 A-scan per second. Eye-tracking system minimized the eye motion artifacts and enabled all scans to be centered on fovea. Detailed information and operational methods were described and validated in our previous study [28]. Each participants' axial length was put into the SS-OCT prior to the scan, and SS-OCT adjusted its scan

area according to the differences in magnification. Both images and analysis including thickness and vascularity were based on axial length calibration. All the images were taken by the same experienced examiner, and all participants maintained their gaze at the internal fixation point, with the chin on the chin rest and forehead firmly against the forehead bar to ensure no head rotation. The signal strengths of structural OCT and OCTA must be > 8, and images should be generally centered on fovea. If not, re-capture would be necessary. Retinal thickness (RT) was determined as the distance between the internal limiting membrane and retinal pigment epithelium-Bruch's membrane (RPE-BM) complex, whereas choroidal thickness (ChT) was determined as the distance between the RPE-BM complex and the choroid-sclera interface. As for vascular features, radical peripapillary capillary plexus (RPCP) vessel density, superficial vascular plexus (SVP) vessel density, intermediate capillary plexus (ICP) vessel density, deep capillary plexus (DCP) vessel density, and choriocapillaris (CC) density were detected. RPCP vessel density was defined from the 5 um above ILM to the interface between nerve fiber layer (NFL) and ganglion cell layer (GCL). SVP vessel density was defined

from the interface of NFL and GCL to two-thirds of the GCL and inner plexiform layer (IPL); DCP vessel density was defined from half of the inner nuclear layer (INL) to 25 um below the lower border of the outer plexiform layer (OPL), and ICP was situated between the layers of SVP and DCP. The area of CC was defined from the based border of RPE-Bruch's membrane complex to the ending at approximately 20 um beneath it (Fig. 1). All these values were presented with a topographic map composed of three concentric circles centered on the central fovea, except RPCP in the inner circle. The inner circle has a diameter of 1 mm. The intermediate circle has a diameter of 3 mm, and the outer circle has a diameter of 6 mm.

Macular Curvature Analysis

We imported the OCT images into an automated layer segmentation software (OCTExplorer, developed by Retinal Image Analysis Lab, Iowa Institute for Biomedical Imaging, Iowa City, IA) [29–31]. OCT image segmentation was reviewed by two independent ophthalmologists (Y.Wu and X.T. Wang). The thinnest part of the macula in the image was defined as the location of the
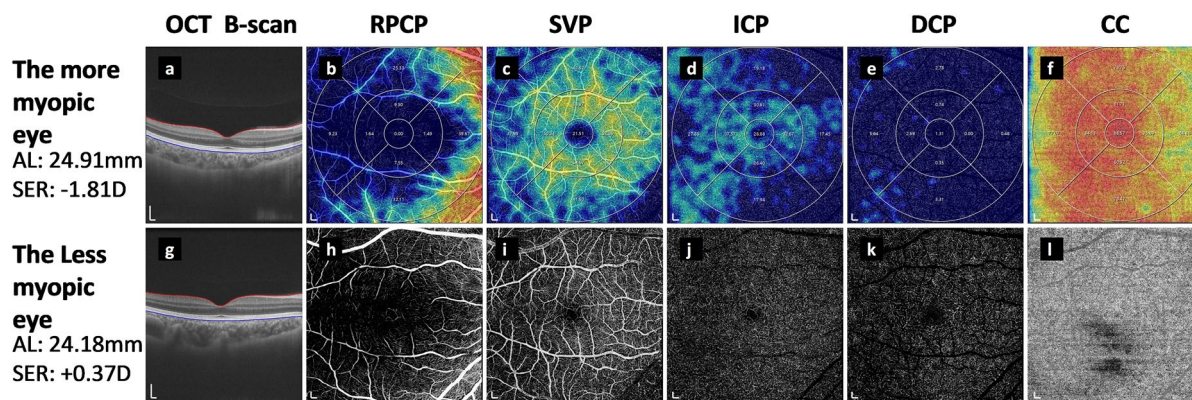

Fig. 1 Representative OCT and OCTA images of the more myopic and the less myopic eyes. **a, g** OCT image of the macula. **b, h** OCTA image of RPCP. **c, i** OCTA image of SVP. **d, j** OCTA image of ICP. **e, k** OCTA image of DCP. **f, l** OCTA image of CC. **a–f** Images captured from the more myopic eye and **g–l** the less myopic eye of the same children with anisomyopia. The values of the microcirculation parameters in three concentric circles (1 mm, 3 mm, 6 mm diameter) were calculated automatically by the system and are illustrated in (**b–f**). Bar = 200 um. *OCT* optical coherence tomography, *OCTA* OCT angiography, *RPCP* radical peripapillary capillary plexus, *SVP* superficial vascular plexus, *ICP* intermediate capillary plexus, *DCP* deep capillary plexus, *CC* choriocapillaris, *AL* axial length, *SER* spherical equivalent refraction

fovea (one array with two elements representing 2D coordinates [x, y] for each subject), and the retinal pigment epithelium (RPE)-Bruch's membrane (BM) was automatically segmented within each axial B-scan. Then, we obtained 20 central slices of horizontal and vertical B-scans passing through the foveal center to generate horizontal and vertical MCIs. The location of RPE-BM boundaries was then extracted and loaded into MATLAB 2022R (The Mathworks Inc., Natick, MA, USA). Here, we used validated polynomial curve fitting method following Müller's approach to generate the estimates of the curvature parameter [19]. Briefly, two-dimensional polynomial curve, denoted as $f(x) = ax^2 + bx + c$, was fitted on the central 20 horizontal and vertical slices to the retrieved RPE-BM boundary seperately. We included slices in the proximity of the fovea to reduce the matching uncertainty, and the average coefficient of the leading term (denoted as "a") was utilized to describe the macular curvature index (MCI). By calculating the leading term of these three curves, it was possible to detect the overall opening size of macula in three concentric circles. Fitting distances of 86, 256, and 512 pixels along each RPE-BM boundary were used for curve fitting, and the corresponding MCIs were referred to curvatures of a 1-mm-diameter circle, 3-mm-diameter circle, and 6-mm-diameter circle at the fovea. A schematic illustration of MCI in shape analysis is described as Fig. 2. The OCT-derived curve fitting was performed on the pixel coordinates.

Finally, nine macular curvature indexes were calculated: 1-mm horizontal/vertical/average MCI, 3-mm horizontal/vertical/average MCI, 6-mm horizontal/vertical/average MCI. The average of the horizontal and vertical MCIs for each region is the average MCI.

Validation of Curvature Measurement

To validate the macular curvature analysis, reliability, repeatability, and agreement of the curve fitting were assessed. First, R^2 is a statistical measure that indicates how well the data fit the regression line, while root-mean-square deviation (RMSD) measures the deviation between the predicted and actual values. Small RMSD (0.656±0.490, 1.030±0.472 and 2.355±1.184 for MCI in 1-mm-, 3-mm-, and 6-mm-diameter circles at fovea) and large R^2 (all 1.00 for MCI in 1-mm-, 3-mm-, and 6-mm-diameter circles at fovea) indicated a superb and reliable matching. Second, foveal center location and curvature measurement were accomplished automatically by the algorithm, ensuring a high level of reproducibility. Moreover, two independent experienced ophthalmologists were asked to segment the RPE-BM boundaries manually, and the intraclass correlation coefficient of 6-mm MCI between human and algorithm was 0.948 (95% CI: 0.925–0.965), indicating high consistency of the manual and machine results.

Statistical Analysis

The statistical analysis was performed by SPSS statistics 23.0 (IBM, Armonk, NY, USA). Data were presented in mean ± standard deviations (SD) unless otherwise stated. Kolmogorov-Smirnov test was used to examine the normality of distribution. Paired Student t-test was used to compare the intraocular difference between more and less myopic eyes for ocular biometrics, retinal and choroid characteristics. Repeated-measure ANOVAs (RM-ANOVAs) were performed to assess the difference in topographic regions in fellow eyes, and least significant difference (LSD) multiple comparisons were used to assess the pairwise differences. Pearson's correlation and partial Pearson's correlation were used to analyze the relationship among MCI, AL, SER, and macular microvascularity (including RPCP, SVP, ICP, DCP, and CC). Then, stepwise linear regression analysis was performed to further determine the associated characteristics of MCI. $P < 0.05$ was considered to be statistically significant.

RESULTS

General Characteristics

A total of 52 participants consisting of 19 males and 33 females (mean age = 12.09, range 7–17 years old) were enrolled in this study. Median height was 157.5 (range 125–180) cm,
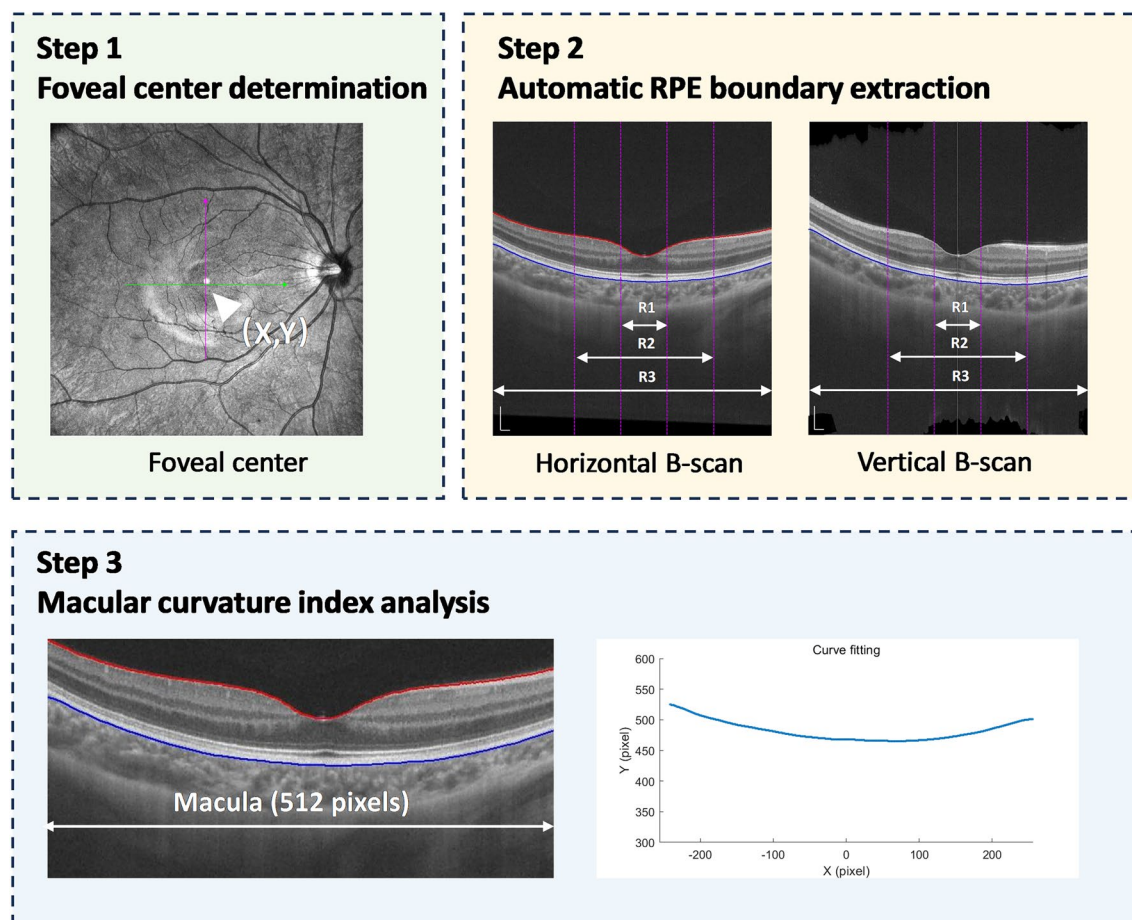
Fig. 2 Schematic illustration of macular curve fitting methodology. (1) Foveal center (white arrow) determination. (2) Central horizontal and vertical cross-section images passing through the foveal center were recognized. RPE boundary was extracted automatically (blue lines). Macular region was divided to three concentric circles in this study (R1: 1-mm-diameter circle at fovea, R2: 3-mm-diameter circle at fovea, R3: 6-mm-diameter circle at fovea). (3) OCT images were processed under the MAT-LAB environment, and the macular contour was fitted into a two-dimensional polynomial curve. *RPE* retinal pigment epithelium. Bar = 200 um

and median BMI was 18.92. The mean SER was − 2.94 ± 1.49 D in more myopic eyes and − 0.36 ± 1.57 D in the less myopic eyes. The demographic and general ocular parameters of the more myopic eyes and less myopic eyes are presented in Supplementary Table 1. No statistical differences were observed in corneal diameter, central corneal thickness (CCT), and intraocular pressure (IOP) ($p > 0.05$). Compared to the less myopic eyes, the mean AL (24.68 ± 0.95 mm vs 23.60 ± 1.01 mm) and ACD (3.27 ± 0.25 mm vs 3.19 ± 0.27 mm) were significantly longer in the more myopic eyes ($p < 0.05$). Pearson's correlation showed SER was highly correlated with AL ($r = -0.739$, $p < 0.001$), and the intraocular difference of SER was highly correlated with AL differences, indicating that the asymmetry in AL explained the main differences in refractive status ($r = -0.716$, $p < 0.001$).

As for the morphological and vascular parameters in macula (seen in Supplementary Table 2), the myopic eyes tended to have thinner macular RT and thinner macular ChT than the less myopic eyes in 1-mm-, 3-mm-, and 6-mm-diameter circle. Moreover, the more myopic eyes had a lower density of ICP and DCP vessels in three concentric circles (all $p < 0.05$) except DCP in the 1-mm circle

($p = 0.184$). No significant differences were found between fellow eyes in RPCP, SVP, and CC density ($p > 0.05$).

Macular Curvature Characteristics in Children with Anisomyopia and its Topographic Features

Comparing between the fellow eyes among children with anisomyopia, the more myopic eyes had on average steeper macula in 1-mm-, 3-mm-, and 6-mm-diameter circles (all $p < 0.001$) than the less myopic eyes (Table 1). When comparing between horizontal and vertical direction, the horizontal MCI was larger than the vertical no matter whether in the more or the less myopic eyes in 1-mm-diameter circle, 3-mm-diameter circle, and 6-mm-diameter circle (all $p < 0.05$).

For the topographic features of macular curvature, curvatures in 1-mm-, 3-mm-, and 6-mm-diameter circles were compared in both horizontal and vertical direction by RM-ANOVAs. The sphericity test results demonstrated statistical significance ($p < 0.001$) along both horizontal and vertical meridians, requiring use of the Greenhouse-Geisser correction method. For horizontal scans, the main effects of eyes and regions were both significant ($F = 129.385$, $p < 0.001$ for eyes; $F = 62.553$, $p < 0.001$ for regions), whereas the interaction effect of eyes and regions on MCI was not significant ($p = 0.702$). Notably, there was a stepwise increase of curvature in these three concentric zones, progressing from 1-mm-, 3-mm-, to 6-mm-diameter circles, indicating a general steepening of the macula. Post hoc multiple comparison of LSD tests showed that curvature in the 6-mm circle was significantly higher than that in the 3-mm region ($p < 0.001$) and 1-mm region ($p < 0.001$) (Fig. 3a). As for vertical scans, the main effect of eyes and regions on MCI was also significant ($F = 65.007$, $p < 0.001$ for eyes; $F = 30.048$, $p < 0.001$ for regions); meanwhile, the interaction effects of eyes and regions were not significant ($p = 0.071$). A similar and significant increasing trend was found among three regions ($p < 0.001$) (Fig. 3b). An illustrative example of variations in MCI can be found in Fig. 4.

Table 1 Macular curvature index in the more myopic and less myopic eyes of children with anisomyopia

| Parameter	More myopic eyes	Less myopic eyes	*P* value
Average MCI ($\times 100$)			
1-mm-diameter circle	0.063 ± 0.072	-0.008 ± 0.056	< 0.001
3-mm-diameter circle	0.112 ± 0.048	0.038 ± 0.044	< 0.001
6-mm-diameter circle	0.121 ± 0.042	0.045 ± 0.039	< 0.001
Horizontal MCI ($\times 100$)			
1-mm-diameter circle	0.076 ± 0.063	0.005 ± 0.072	< 0.001
3-mm-diameter circle	0.130 ± 0.047	0.048 ± 0.058	< 0.001
6-mm-diameter circle	0.131 ± 0.044	0.051 ± 0.047	< 0.001
Vertical MCI ($\times 100$)			
1-mm-diameter circle	0.050 ± 0.114	-0.021 ± 0.083	< 0.001
3-mm-diameter circle	0.094 ± 0.061	0.028 ± 0.053	< 0.001
6-mm-diameter circle	0.110 ± 0.046	0.040 ± 0.043	< 0.001

MCI macular curvature index
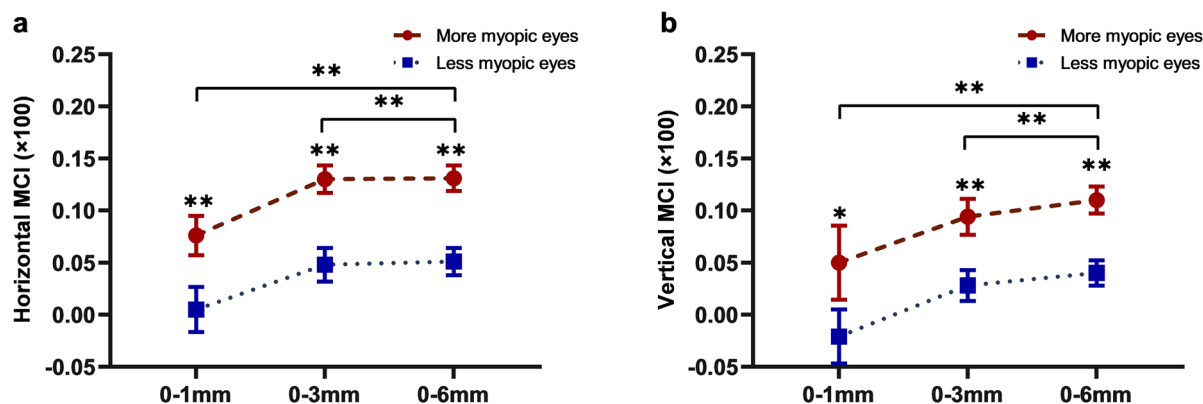
Fig. 3 Topographic curvature analysis in eyes of children with anisomyopia. Comparison of MCI in 1-mm-, 3-mm-, and 6-mm-diameter circles in horizontal (**a**) and vertical (**b**) meridians. MCI: macular curvature index. Data were expressed as means and 95% confidence interval. Two-way repeated measure ANOVA, $p < 0.05^*$, $p < 0.001^{**}$
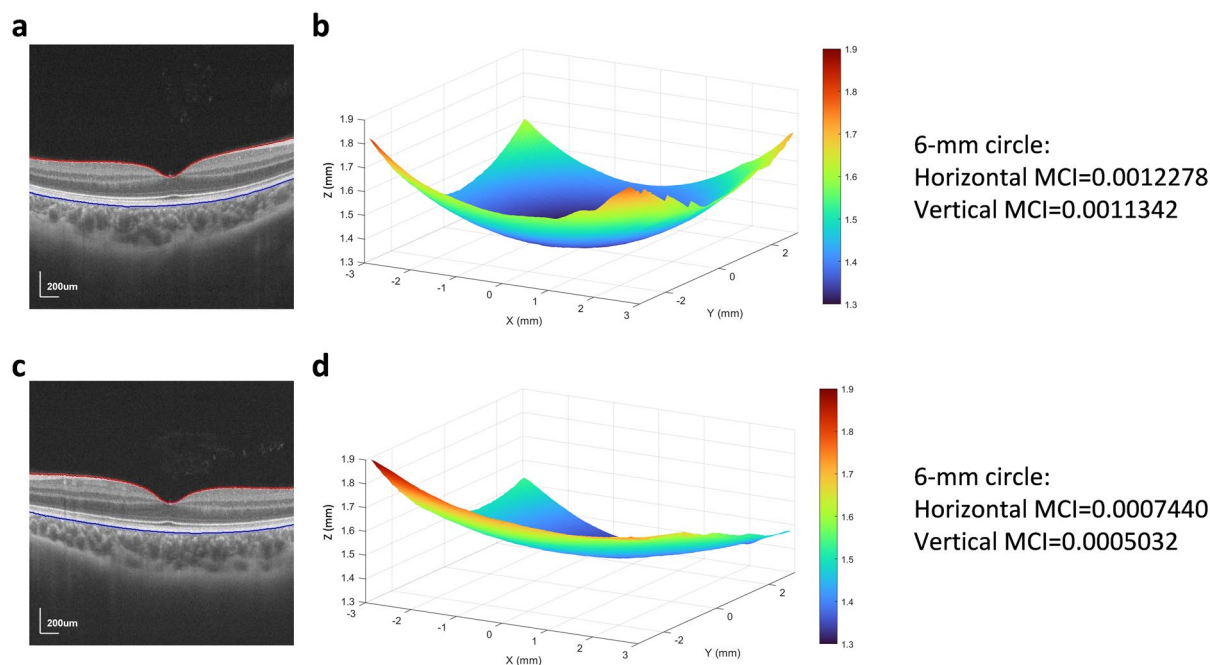

Fig. 4 Representative OCT images; the corresponding three-dimensional macular morphology and topographic curvature map of fellow eyes in one child with anisomyopia. In the more myopic eye, macula was steeper and MCI was larger (**a**, **b**) compared to the less myopic eye (**c**, **d**). The horizontal OCT scans in the more myopic eye and less myopic eye are shown in (**a**, **c**). Three-dimensional morphological maps of retinal pigment epithelium boundary in the more myopic eye and less myopic eye as well as its MCI are shown in **b**, **d**, respectively. OCT: optical coherence tomography; MCI: macular curvature index. Bar = 200 um

Table 2 Correlation between MCI, AL and SER in children with anisomyopia

Parameter	AL		SER	
	r	p	r	p
1-mm-diameter circle				
Horizontal MCI	0.417	< 0.001	− 0.350	< 0.001
Vertical MCI	0.079	0.426	− 0.091	0.358
Average MCI	0.272	0.005	− 0.246	0.012
3-mm-diameter circle				
Horizontal MCI	0.492	< 0.001	− 0.435	< 0.001
Vertical MCI	0.222	0.024	− 0.258	0.008
Average MCI	0.403	< 0.001	− 0.390	< 0.001
6-mm-diameter circle				
Horizontal MCI	0.524	< 0.001	− 0.519	< 0.001
Vertical MCI	0.383	< 0.001	− 0.418	< 0.001
Average MCI	0.484	< 0.001	− 0.500	< 0.001

MCI macular curvature index, *AL* axial length, *SER* spherical equivalent refraction

Moreover, correlation analysis demonstrated positive correlation of AL and myopic SER with the average MCI in three regions, and indicated a stronger correlation of MCI with AL instead of myopic SER. Horizontally, the 1-mm, 3-mm, and 6-mm MCIs were significantly correlated with AL and SER; however, similar correlation only exists in 3-mm- and 6-mm-diameter circles in vertical direction. Stronger correlation of horizontal MCI with myopic severity than vertical MCI was found (Table 2). No significant correlations between age and horizontal, vertical, and average MCI were found (all $p > 0.05$). Overall, the more myopic eyes exhibited steeper macula than the less myopic eyes. Horizontal MCI in 6-mm-diameter circles was the highest in the more myopic eyes and was the parameter most relevant to myopic severity, providing a more effective and comprehensive representation of macular morphology.

Correlation Between MCI and Macular Microvascularity in Retina and Choroid

Partial correlation coefficients between MCI and macular microvascularity adjusted for AL are summarized in Fig. 5 and Supplementary Table 3. Specifically, a significant negative correlation was observed only between MCI and the microvascularity of DCP density, after accounting for AL ($r = - 0.329$, $p^* = 0.016$). RPCP ($r = 0.151$, $p^* = 0.677$) and SVP ($r = - 0.037$, $p^* = 0.929$) density remained unchanged, and ICP density ($r = - 0.213$, $p^* = 0.386$) showed a negative but not significant correlation with MCI. No significant correlation was observed between the CC density and MCI ($p > 0.05$), indicating that this relationship may be specific to the retinal DCP rather than extending to the choroidal vasculature.
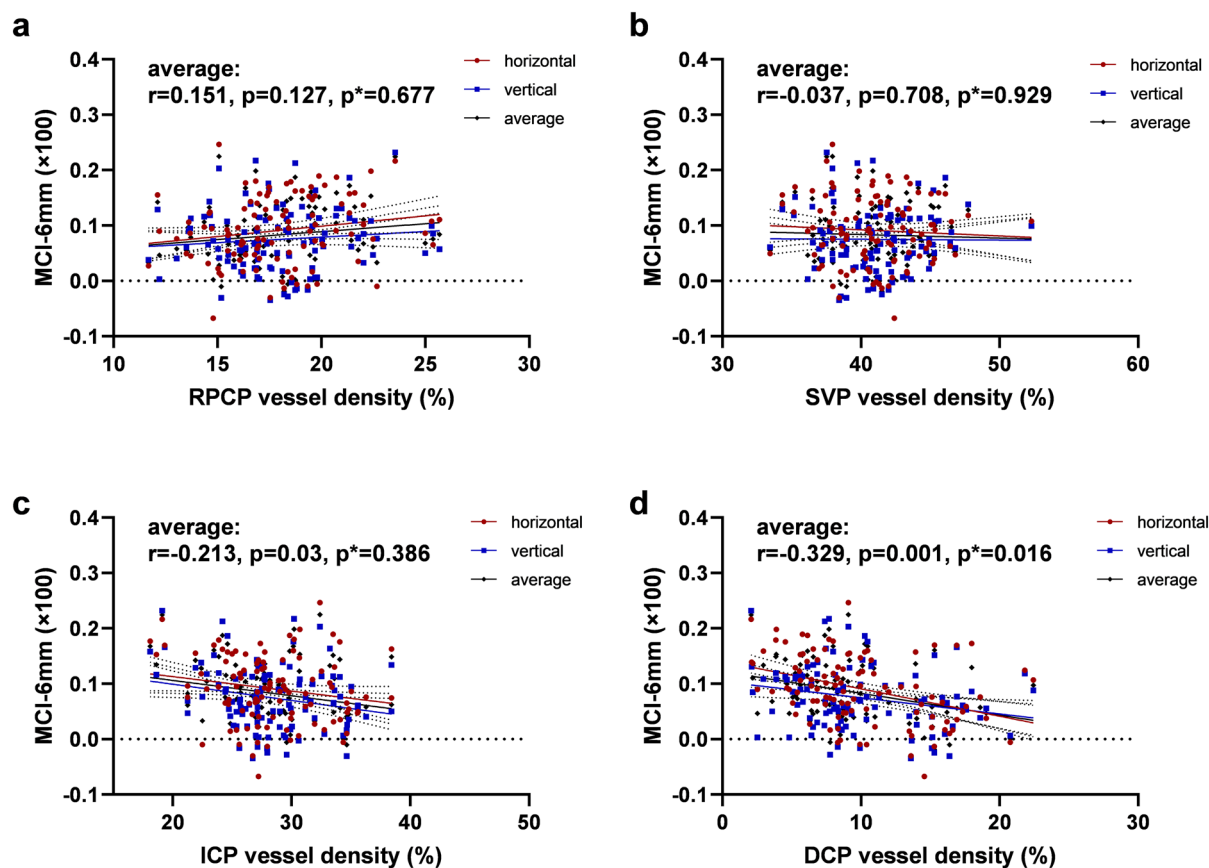
Fig. 5 Scatter plot showing correlation between macular curvature and retinal microvascularity in children with anisomyopia. **a** Correlation between RPCP vessel density and 6-mm MCI. **b** Correlation between SVP vessel density and 6-mm MCI. **c** Correlation between ICP vessel density and 6-mm MCI. **d** Correlation between DCP vessel density and 6-mm MCI. *p p* value by Pearson's correlation, *p* p* value after adjusting the axial length by partial correlation. The dashed lines are the 95% confidence intervals for the regression line. *RPCP* radical peripapillary capillary plexus, *SVP* superficial vascular plexus, *ICP* intermediate capillary plexus, *DCP* deep capillary plexus, *MC*: macular curvature index.

Table 3 Stepwise multiple linear regression between MCI (× 100) in 6-mm-diameter circle and ocular parameters

Variables	Average MCI			Horizontal MCI			Vertical MCI		
	B	β	p	B	β	p	B	β	p
AL	0.0177	0.3555	< 0.001	0.0204	0.3719	< 0.001	0.0197	0.3827	< 0.001
DCP vessel density	− 0.0022	− 0.1850	0.037	− 0.0029	− 0.2203	0.009	–	–	–
ChT	− 0.0001	− 0.1888	0.045	− 0.0002	− 0.2211	0.014	–	–	–

MCI macular curvature index, *AL* axial length, *DCP* deep capillary plexus, *ChT* choroidal thickness

Factors Associated with MCI in 6-mm-Diameter Circle

To identify the independent factors associated with MCI in 6-mm-diameter circles, stepwise multiple linear regression analysis in all subjects was performed. Age, gender, IOP, AL, and the retinal and choroidal structural and vascular parameters were put in the model. The results, as presented in Table 3, showed the association of average, horizontal, and vertical MCI with each explored covariate within the final regression model. On average, greater MCI was independently associated with longer AL ($\beta = 0.3555$,

$p < 0.001$), smaller ChT ($\beta = -0.1888$, $p = 0.045$), and reduced DCP vascular density ($\beta = -0.185$, $p = 0.037$). According to the model, for every 1 mm increase in AL, average MCI increased by 0.000177. Results of standardized β indicated that AL vascular density makes the greatest contribution to horizontal MCI, followed by ChT and DCP. Other systemic variables including age, gender, IOP, and ocular variables including RT, RPCP, SVP, ICP, and CC have no significant correlation with MCI (all $p > 0.05$). For horizontal MCI, AL, DCP, and ChT were its independent factors, while for vertical MCI, only AL was its independent factor.

Table 4 Summary of previous studies on macular curvature in myopic eyes

Study	Age (Years)	Myopia severity	Methods	Mathematical principle	Curvature changes and associated factor
Wakazono et al. [25]	67.7 ± 9.8	AL: 29.9 ± 2.2	SD-OCT	Differential equation	Curvature within 6-mm-diameter circle: MTM > simple HM; Curvature within 6–12-mm-diameter ring: simple HM > MTM
Wakazono et al. [20]	63.4 ± 13.8	AL: 28.47 ± 1.88	SD-OCT	Differential equation	Longitudinal curvature change correlated with gender, AL, and baseline curvature
Numa et al. [23]	57.3 ± 13.6	AL: 24.14 ± 1.42	SD-OCT	Differential equation	Mean curvature correlated with gender, age and AL
Miyake et al. [22]	61.9 ± 14.1	AL: 28.68 ± 1.74	SD-OCT	Differential equation	Mean curvature: HM with PS > simple HM; variance of curvature: HM with PS > simple HM
Park et al. [32]	60.7 ± 9.1; 60.0 ± 10.6; 52.3 ± 9.1 for MTM, mCNV and simple HM	AL: 29.8 ± 1.7; 30.0 ± 1.4; 29.5 ± 1.5 for MTM, mCNV and simple HM	SD-OCT	Polynomials	Curvature: MTM > simple HM > mCNV
Müller et al. [19]	57.3 ± 8.11	SER: -0.320 ± 2.680	SD-OCT	Polynomials	Horizontal curvature correlated with SER, age, gender, race, etc.
Kuo et al. [33]	23 ± 3	SER: EM: -0.03 ± 0.36D; HM: -8.08 ± 1.40D	MRI	Polynomials	Horizontal curvature correlated with relative peripheral refraction
Breher et al. [34]	24.5 ± 3.5	SER: -1.33 ± 1.83	SS-OCT	Spherical fit	Horizontal curvature correlated with AL
Minami et al. [21]	43.2 ± 19.8	SER: -2.6 ± 2.5	SS-OCT	Cubic spline interpolation	Horizontal curvature associated with AL and choroidal thickness

AL axial length, *SER* spherical equivalent refraction, *SD-OCT* spectral domain-OCT, *SS-OCT* swept source-OCT, *MRI* magnetic resonance imaging, *MTM* myopic tractional maculopathy, *mCNV* myopic choroidal neovascularization, *HM* high myopia, *EM* emmetropia, *PS* posterior staphyloma

DISCUSSION

Alterations in retinal shape are associated with the development of myopia, but many details remain unclear. The present study evaluated MCI in a unique group, children with anisomyopia, to test for the relationship between MCI and myopia. To our knowledge, this is the first study to investigate the relationship between curvature and macular microvasculature in children. MCI was greater in the more myopic eyes compared with less myopic eyes. MCI has a stronger correlation with AL than SER, especially in horizontal compared with vertical. Eyes with larger MCI presented with smaller DCP density. AL, DCP density, and ChT were independent factors associated with MCI in 6-mm-diameter circles. We recommended MCI of OCT scans to evaluate the macular morphology as well as act as an early indicator of microvascularity loss, and it could be a valuable metric for myopia assessment in clinical practice.

Myopic eyes are not simply elongated but also become out-pouched in the posterior pole. By utilizing the special design of self-control in anisomyopes, the present study found that, in children without high myopia, the more myopic eyes had larger MCI than the less myopic eyes, and there was a positive correlation among AL, SER, and MCI. This finding suggests that an increase in MCI in the more myopic eyes may represent a potential adaptive response to axial elongation in children without high myopia. Some previous studies reporting the macular curvature-related changes are summarized as Table 4. Shogo Numa et al. first reported a significant correlation between OCT-based macular curvature and AL in middle-aged adults from a Japanese community-based cohort [23]. This correlation was further supported by Wakazono T et al. with the same methodology [20]. They also highlighted the utility of macular curvature measurements in predicting the onset of myopic traction maculopathy. In a recent study within the UK Biobank, higher MCI value among adults was associated with higher myopia severity [19] apart from age, gender, or ethnicity. However, most of them only included the adults with high myopia and pathological myopia. Our results

extended these findings to a pediatric population, suggesting the presence of a steeper macula in human myopia even at the early stage of non-high myopia. We proposed that a higher MCI value would be an indicator of macular morphology and myopia severity in children.

Notably, MCI was larger in horizontal than vertical directions, indicating that the myopic eyes were longitudinally elongated ellipses with a slightly flatter curvature in vertical than horizontal dimension. The significant differences in horizontal MCI among 1-mm, 3-mm, and 6-mm circles also indicated that myopic eyes became steeper in horizontal than vertical direction. This observation aligned with Atchison et al.'s MRI study, which reported that when emmetropic eyes shifted to myopia, more changes occurred in axial (0.35 mm/D) than in vertical height (0.19 mmm/D, i.e., superior/inferior side) and even less in horizontal width (nasal/temporal side) [10]. The mechanism underlying this horizontal-vertical difference is unclear. One possible explanation is the influence of extra-ocular anatomical factors. Zielinski et al. observed a larger cross-sectional area of lateral rectus muscle in highly myopic eyes compared to emmetropic eyes [35]. The increased mechanical pressure against the temporal sclera by thicker lateral rectus muscle may restrict the horizontal expansion, thereby contributing to a higher horizontal MCI. Another possible explanation is that MCI changes could be driven by optical mechanisms. Both human studies and animal experiments confirmed that the peripheral defocus played an important role in myopia development. Studies have indicated that myopic individuals exhibit temporal-nasal asymmetric retina as well as more hyperopic relative peripheral refraction along the horizontal meridian [36, 37]. An increase in horizontal MCI could influence peripheral refraction. In turn, unbalanced optical signals from asymmetric peripheral vision could further contribute to the curvature change, and changes in peripheral refraction could reshape the retina [38–40]. Overall, it appears that eye growth in myopes is non-coordinated, with horizontal MCI responding more actively to visual stimulus and correlating more closely with myopia severity.

So far, few studies have investigated the relationship between MCI and macular microvascularity. From a biomechanical perspective, mechanical stress and perfusion impairment are interconnected [41]. Our finding of the negative association between MCI values (average, horizontal and vertical) and DCP density indicated that myopic macula with larger MCI may be under greater mechanical stretching and strain, in which capillaries may be more prone to compression. Interestingly, in our study, among all the microvascular parameters in macula, DCP density was most associated with the MCI changes related to myopia, compared to RPCP, SVP, and ICP. On the one hand, the fragile, small-diameter vessels of the DCP are more easily straightened and disrupted than the large retinal vessels in the SVP which are directly connected to retinal arterioles. On the other hand, the mechanical strain in different retinal sublayers may vary under the same MCI. Studies have indicated a general trend of increasing retinal layer stiffness from the ganglion side to the photoreceptor side [42]. Qu et al. found the stiffness of the outer retina (inner nuclear and outer plexiform layer) was almost 2–3 times larger than the inner retina (nerve fiber and ganglion cell layer) in in vitro and vivo animal models [43, 44]. To achieve the same extent of deformation, the stiffer sublayer where DCP is positioned will experience larger mechanical strain. The observed relationship between changes in MCI and the decrease in DCP density, especially when other retinal sublayer vessel density has not yet shown similar declines, not only strengthened the understanding of the spatiotemporal adaptations occurring in the retina but also suggested MCI as an early indicator of early changes within the retina's microvascular network in children.

Moreover, DCP contributes part of the oxygen demand (10–15%) and nutrition necessary for the inner photoreceptor segments. Hypoperfusion of the DCP may lead to hypoxia and nutritional deficiency in these layers [45, 46]. Studies have reported that decreased DCP density was related to the structural impairment in outer retina [47]. Our results also showed that DCP density was one of the independent associated factors for horizontal MCI after adjusting for confounders, yet the role it played in MCI was unknown. Further studies are needed to clarify the mechanisms behind these findings.

Several limitations of this study should be noted. First, it is a cross-sectional study, providing only evidence for a correlation between macular curvature and myopia. Future longitudinal studies are needed to investigate its association with myopia progression and microvascularity changes. Second, we focused on the horizontal and vertical OCT scans, which could miss some changes in the radial scans; three-dimensional curvature analysis may provide more information for further evaluation. Third, the sample size is relatively small; nevertheless, post hoc power analysis with G-power software based on MCI indicated a > 95% detection power [48]. Therefore, it is still sufficient to determine the curvature differences in children with anisomyopia. Notably, the described curvature index is not considered an absolute curvature (unit:mm^{-1}) because of the uncorrected optical distortion from parallel OCT B-scan assembly, which may result in a flatter shape in contrast to that obtained through MRI [49, 50], and the unit is different for them. However, distortion in our images should have led to fewer curvature measures in longer eyes and vice versa in shorter eyes, and conclusions from our analysis should not be altered. More importantly, this study placed more emphasis on the potential clinical application of MCI in OCT images in the myopia assessment in children, and MCI can still be considered a clinically appropriate approach in daily practice.

CONCLUSION

In conclusion, our study demonstrated that MCI was a valuable metric for myopia assessment. Using OCT, we found larger MCI in the more myopic than less myopic eyes in children with anisomyopia. Furthermore, larger MCI was associated with smaller DCP density, and DCP density was one of the independent factors associated with average and horizontal MCI. Quantitative assessment of MCI is of great importance

and clinically applicable for assessing myopia, suggesting early myopia-related changes within the retina's microvascular network in children. Further longitudinal investigation on school-aged children is needed to find its role in early detection and monitoring of myopia progression.

Data Availability. The data that support the findings of this study are available from the corresponding author upon reasonable request. Supplementary information is available for this paper.

Declarations

Conflict of Interest. Yue Wu, Xin Liu, Yuying Liu, Wenzhe Qian, Liandi Huang, Yixiang Wu, Xuetong Wang, Ying Yuan, and Bilian Ke have nothing to disclose.

Ethical Approval. Written informed consent was obtained from all the children and their guardians. The study protocol was approved by ethics committee of Shanghai General Hospital, Shanghai Jiao Tong University (approval number 2022KY038), and was conducted in accordance with the Helsinki Declaration.

REFERENCES

1. Baird PN, Saw SM, Lanca C, Guggenheim JA, Smith Iii EL, Zhou X, et al. Myopia. Nat Rev Dis Primers. 2020;6(1):99.

2. Holden BA, Fricke TR, Wilson DA, Jong M, Naidoo KS, Sankaridurg P, et al. Global prevalence of myopia and high myopia and temporal trends from 2000 through 2050. Ophthalmology. 2016;123(5):1036–42.

3. Ohno-Matsui K, Akiba M, Modegi T, Tomita M, Ishibashi T, Tokoro T, et al. Association between shape of sclera and myopic retinochoroidal lesions in patients with pathologic myopia. Invest Ophthalmol Vis Sci. 2012;53(10):6046.

4. Ikuno Y. Overview of the complications of high myopia. Retina. 2017;37(12):2347–51.

5. Ueda E, Yasuda M, Fujiwara K, Hashimoto S, Ohno-Matsui K, Hata J, et al. Five-year incidence of myopic maculopathy in a general japanese population: the Hisayama Study. JAMA Ophthalmol. 2020;138(8):887.

6. Leveziel N, Marillet S, Dufour Q, Lichtwitz O, Bentaleb Y, Pelen F, et al. Prevalence of macular complications related to myopia - results of a multicenter evaluation of myopic patients in eye clinics in France. Acta Ophthalmol. 2020;98(2):e245–51.

7. Moriyama M, Ohno-Matsui K, Hayashi K, Shimada N, Yoshida T, Tokoro T, et al. Topographic analyses of shape of eyes with pathologic myopia by high-resolution three-dimensional magnetic resonance imaging. Ophthalmology. 2011;118(8):1626–37.

8. Yan YN, Wang YX, Yang Y, Xu L, Xu J, Wang Q, et al. Ten-year progression of myopic maculopathy. Ophthalmology. 2018;125(8):1253–63.

9. Matsumura S, Kuo AN, Saw SM. An update of eye shape and myopia. Eye Contact Lens. 2019;45(5):279–85.

10. Atchison DA, Jones CE, Schmid KL, Pritchard N, Pope JM, Strugnell WE, et al. Eye shape in emmetropia and myopia. Invest Ophthalmol Vis Sci. 2004;45(10):3380.

11. Tabernero J, Schaeffel F. More irregular eye shape in low myopia than in emmetropia. Invest Ophthalmol Vis Sci. 2009;50(9):4516.

12. Lim LS, Yang X, Gazzard G, Lin X, Sng C, Saw SM, et al. Variations in eye volume, surface area, and shape with refractive error in young children by magnetic resonance imaging analysis. Invest Ophthalmol Vis Sci. 2011;52(12):8878.

13. Feng J, Wang R, Yu J, Chen Q, He J, Zhou H, et al. Association between different grades of myopic tractional maculopathy and OCT-based macular scleral deformation. JCM. 2022;11(6):1599.

14. Zhou ZH, Xiong PP, Sun J, Wang YL, Wang JL. Effects of posterior staphyloma on choroidal structure in myopic adults: a retrospective study. BMC Ophthalmol. 2023;23(1):406.

15. Hwang YH, Kim YY. Macular thickness and volume of myopic eyes measured using spectral-domain optical coherence tomography. Clin Exp Optom. 2012;95(5):492–8.

16. Zhang Z, He X, Zhu J, Jiang K, Zheng W, Ke B. Macular measurements using optical coherence tomography in healthy Chinese school age children. Invest Ophthalmol Vis Sci. 2011;52(9):6377–83.

17. Komori S, Ueno S, Ito Y, Sayo A, Meinert M, Kominami T, et al. Steeper macular curvature in eyes with non-highly myopic retinitis pigmentosa. Invest Ophthalmol Vis Sci. 2019;60(8):3135.

18. Chen C, Du R, Xie S, Lu H, Xiong J, Wang Y, et al. Longitudinal study of changes in inner scleral curvature patterns and development of posterior staphylomas in highly myopic eyes of children and adolescents. Retina. 2023;43(3):454–63.

19. Müller PL, Kihara Y, Olvera-Barrios A, Warwick AN, Egan C, Williams KM, et al. Quantification and predictors of OCT-based macular curvature and dome-shaped configuration: results from the UK Biobank. Invest Ophthalmol Vis Sci. 2022;63(9):28.

20. Wakazono T, Yamashiro K, Miyake M, Hata M, Miyata M, Uji A, et al. Time-course change in eye shape and development of staphyloma in highly myopic eyes. Invest Ophthalmol Vis Sci. 2018;59(13):5455–61.

21. Minami S, Ito Y, Ueno S, Kataoka K, Takeuchi J, Ito H, et al. Analysis of macular curvature in normal eyes using swept-source optical coherence tomography. Jpn J Ophthalmol. 2020;64(2):180–6.

22. Miyake M, Yamashiro K, Akagi-Kurashige Y, Oishi A, Tsujikawa A, Hangai M, et al. Analysis of fundus shape in highly myopic eyes by using curvature maps constructed from optical coherence tomography. Bui BV, editor. PLoS ONE. 2014;9(9): e107923.

23. Numa S, Yamashiro K, Wakazono T, Yoshikawa M, Miyake M, Nakanishi H, et al. Prevalence of posterior staphyloma and factors associated with its shape in the Japanese population. Sci Rep. 2018;8(1):4594.

24. Ikuno Y, Jo Y, Hamasaki T, Tano Y. Ocular risk factors for choroidal neovascularization in pathologic myopia. Invest Ophthalmol Vis Sci. 2010;51(7):3721.

25. Wakazono T, Yamashiro K, Miyake M, Nakanishi H, Oishi A, Ooto S, et al. Association between eye shape and myopic traction maculopathy in high myopia. Ophthalmology. 2016;123(4):919–21.

26. Wang Y, Chen J, Zhang M, Yu S, Gong Y, Lin F, et al. Genetic factors and characteristics on spectral-domain optical coherence tomography are associated with choroidal thickness in ABCA4-related retinopathy. Retina. 2024;44(1):166–74.

27. Dirani M, Chan YH, Gazzard G, Hornbeak DM, Leo SW, Selvaraj P, et al. Prevalence of refractive error in Singaporean Chinese children: the Strabismus, Amblyopia, and Refractive Error in Young Singaporean Children (STARS) Study. Invest Ophthalmol Vis Sci. 2010;51(3):1348.

28. Liu L, Zhu C, Yuan Y, Hu X, Chen C, Zhu H, et al. Three-dimensional choroidal vascularity index in high myopia using swept-source optical coherence tomography. Curr Eye Res. 2022;47(3):484–92.

29. Abramoff MD, Garvin MK, Sonka M. Retinal Imaging and Image Analysis. IEEE Rev Biomed Eng. 2010;3:169–208.

30. Garvin MK, Abramoff MD, Xiaodong Wu, Russell SR, Burns TL, Sonka M. Automated 3-D intraretinal layer segmentation of macular spectral-domain optical coherence tomography images. IEEE Trans Med Imaging. 2009;28(9):1436–47.

31. Li K, Wu X, Chen DZ, Sonka M. Optimal surface segmentation in volumetric images-a graph-theoretic approach. IEEE Trans Pattern Anal Mach Intell. 2006;28(1):119–34.

32. Park UC, Ma DJ, Ghim WH, Yu HG. Influence of the foveal curvature on myopic macular complications. Sci Rep. 2019;9(1):16936.

33. Kuo HY, Hsiao JCJ, Chen JJ, Lee CH, Chuang CC, Sun HY. The correlations between horizontal and vertical peripheral refractions and human eye shape using magnetic resonance imaging in highly myopic eyes. Healthcare. 2021;9(8):966.

34. Breher K, Ohlendorf A, Wahl S. Myopia induces meridional growth asymmetry of the retina: a pilot study using wide-field swept-source OCT. Sci Rep. 2020;10(1):10886.

35. Zieliński G, Matysik-Woźniak A, Pankowska A, Pietura R, Rejdak R, Jonak K. High myopia and thickness of extraocular and masticatory muscles—7T MRI, preliminary study. JCM. 2023;12(12):4166.

36. Smith EL, Hung LF, Huang J, Arumugam B. Effects of local myopic defocus on refractive development in monkeys. Optom Vis Sci. 2013;90(11):1176–86.

37. Stone RA, Pendrak K, Sugimoto R, Lin T, Gill AS, Capehart C, et al. Local patterns of image degradation differentially affect refraction and eye shape in chick. Curr Eye Res. 2006;31(1):91–105.

38. Zhang HY, Lam CSY, Tang WC, Leung M, To CH. Defocus incorporated multiple segments spectacle lenses changed the relative peripheral refraction: a 2-year randomized clinical trial. Invest Ophthalmol Vis Sci. 2020;61(5):53.

39. Huang Y, Li X, Ding C, Chen Y, Chen H, Bao J. Orthokeratology reshapes eyes to be less prolate and more symmetric. Cont Lens Anterior Eye. 2022;45(4): 101532.

40. Li X, Huang Y, Zhang J, Ding C, Chen Y, Chen H, et al. Treatment zone decentration promotes retinal reshaping in Chinese myopic children wearing orthokeratology lenses. Ophthalmic Physiologic Optic. 2022;42(5):1124–32.

41. Kim JA, Kim TW, Lee EJ, Girard MJA, Mari JM. Relationship between lamina cribrosa curvature and the microvasculature in treatment-naïve eyes. Br J Ophthalmol. 2020;104(3):398–403.

42. He Y, Qu Y, Zhu J, Zhang Y, Saidi A, Ma T, et al. Confocal shear wave acoustic radiation force optical coherence elastography for imaging and quantification of the in vivo posterior eye. IEEE J Sel Top Quantum Electron. 2019;25(1):1–7. https://doi.org/10.1109/JSTQE.2018.2834435.

43. Qu Y, He Y, Zhang Y, Ma T, Zhu J, Miao Y, et al. Quantified elasticity mapping of retinal layers using synchronized acoustic radiation force optical coherence elastography. Biomed Opt Express. 2018;9(9):4054–63.

44. Qu Y, He Y, Saidi A, Xin Y, Zhou Y, Zhu J, et al. In vivo elasticity mapping of posterior ocular layers using acoustic radiation force optical coherence elastography. Invest Ophthalmol Vis Sci. 2018;59(1):455–61.

45. Yao H, Xin D, Li Z. The deep vascular plexus density is closely related to myopic severity. Ophthalmic Res. 2022;65(4):455–65.

46. Lin F, Li F, Gao K, He W, Zeng J, Chen Y, et al. Longitudinal changes in macular optical coherence tomography angiography metrics in primary open-angle glaucoma with high myopia: a prospective study. Invest Ophthalmol Vis Sci. 2021;62(1):30.

47. Ye J, Wang M, Shen M, Huang S, Xue A, Lin J, et al. Deep retinal capillary plexus decreasing correlated with the outer retinal layer alteration and visual acuity impairment in pathological myopia. Invest Ophthalmol Vis Sci. 2020;61(4):45.

48. Faul F, Erdfelder E, Lang AG, Buchner A. G*Power 3: A flexible statistical power analysis program for the social, behavioral, and biomedical sciences. Behav Res Methods. 2007;39(2):175–91.

49. Kuo AN, Verkicharla PK, McNabb RP, Cheung CY, Hilal S, Farsiu S, et al. Posterior eye shape measurement with retinal OCT compared to MRI. Invest Ophthalmol Vis Sci. 2016;57(9):OCT196.

50. Kuo AN, McNabb RP, Chiu SJ, El-Dairi MA, Farsiu S, Toth CA, et al. Correction of ocular shape in retinal optical coherence tomography and effect on current clinical measures. Am J Ophthalmol. 2013;156(2):304–11.